Effects of Printing-Induced Interfaces on Localized Strain within 3D Printed Hydrogel Structures

Kyle Christensen[1,*], Brian Davis[1,*], Yifei Jin[1], Yong Huang[1,2,3,**]

[1]Department of Mechanical and Aerospace Engineering, University of Florida, Gainesville, FL 32611, USA

[2]Department of Biomedical Engineering, University of Florida, Gainesville, FL 32611, USA

[3]Department of Materials Science and Engineering, University of Florida, Gainesville, FL 32611, USA

[*]Equal contribution

[**]Corresponding author, P. O. Box 116250, University of Florida, Gainesville, FL 32611, USA, Phone: 001-352-392-5520, Fax: 001-352-392-7303, Email: yongh@ufl.edu

Abstract

Additive manufacturing, or 3D printing, is a promising approach for the fabrication of biological structures for regenerative medicine applications using tissue-like materials such as hydrogels. Herein, inkjet printing is implemented as a model droplet-based 3D printing technology for which interfaces have been shown to form between printed lines within printed layers of hydrogel structures. Experimental samples with interfaces in two orientations are fabricated by inkjet printing and control samples with and without interfaces are fabricated by extrusion printing and casting, respectively. The formation of partial and full interfaces is modeled in terms of printing conditions and gelation parameters, and an approach to predicting

the ratio of interfacial area to the total contact area between two adjacent lines is presented. Digital image correlation is used to determine strain distributions and identify regions of increased localized deformation for samples under uniaxial tension. Despite the presence of interfaces in inkjet-printed samples, strain distributions are found to be homogeneous regardless of interface orientation, which may be attributed to the multi-layer nature of samples. Conversely, single-layer extrusion-printed samples exhibit localized regions of increased deformation between printed lines, indicating delamination along interfaces. The effective stiffness, failure strength, and failure strain of inkjet-printed samples are found to be dependent on the orientation of interfaces within layers. Specifically, inkjet-printed samples in which tensile forces pull apart interfaces exhibit significantly decreased mechanical properties compared to cast samples.

Keywords: inkjet printing; hydrogel; interfacial deformation; mechanical property; digital image correlation

1. Introduction

Recently, numerous additive manufacturing approaches, in particular, three-dimensional (3D) bioprinting, have successfully been applied to the fabrication of biological structures [1,2]. Bioprinting aims to fabricate biologically relevant structures using tissue-like materials, such as hydrogels, for regenerative medicine applications including pharmaceutical drug screening and organ repair and replacement. Thus far, several bioprinting approaches have been successfully used to fabricate 3D structures layer-by-layer including: inkjet printing [3-5], laser printing [6,7], and extrusion deposition [8-11]. For printed functional structures to be useful for various

biomedical applications, their mechanical behavior must be characterized and fundamentally understood in addition to the evaluation of their biological properties. With the growing interest in 3D bioprinting, there is a need to quantify the effects of interfaces on the mechanical behavior of printed tissue-like structures.

The mechanical behavior and properties of homogeneous soft tissue-like materials have been extensively characterized in various ways including quasi-static tensile testing [12,13], compression testing [14,15], and needle insertion (indentation) [16,17], to name a few. However, the mechanical properties of structures fabricated by typical 3D printing technologies become anisotropic due to the effects of the layer-by-layer fabrication process, such that characterization of bulk structures alone is not sufficient to describe the mechanical behavior of printed structures [18-21]. In particular, decreased bond strength between subsequently printed layers may lead to significant decreases in mechanical properties when tensile forces act to pull apart these layers. Although the mechanical properties of 3D printed soft structures have been investigated on a global scale [9,22-24], little is known about how interfaces between subsequently printed regions affect the mechanical behavior of printed structures locally. In particular, interfacial regions may experience excessive deformation and delamination under tensile loads. In addition, interfaces may also be formed between adjacent features within each printed layer [25], which have been largely ignored during the characterization of printed structures.

The objective of this study is to quantify the effects of printing-induced interfacial features and their orientation within printed layers on strain distributions across printed structures under tension. Similar interfaces are formed between successively printed layers within a 3D structure as gelation of each printed layer is typically complete before subsequent layers are deposited [25]. In this study, inkjet printing has been chosen as a model droplet-based 3D

printing technology for which interfaces have been shown to form between printed lines within a printed layer [25], and adjacent lines within printed layers facilitate the observation of strain distributions of printed layers under deformation. Printed droplets coalesce to form continuous lines along printing paths, but interfaces at which coalescence does not occur may form between adjacent lines depending on the state of gelation of adjacent build materials [25]. As such, the formation and effects of these interfaces on inkjet-printed samples have been investigated herein. For comparison, extrusion printing and casting have been implemented to fabricate samples with and without interfaces, respectively.

In this study, digital image correlation (DIC) has been implemented to determine the local strain distribution within 3D printed hydrogel structures, enabling observation of deformation at interfaces compared to that of bulk structures. DIC is a non-contact, optical method used to determine the displacement and strain field of samples undergoing deformation by tracking the pixel intensity within a specified subset for a reference pattern through sequential images. The principle of DIC is to track a subset of pixels between two or more images captured during loading, and from these images, local displacements can be calculated. DIC has been used to evaluate the deformation of soft tissue-like materials including the investigation of the effect of strain rate on the failure strength [26] and the study of the effect of gelatin concentration on the tensile strength [27].

2. Materials and Methods

2.1. Materials

Sodium alginate has been widely utilized for bioprinting studies [3,5,7,9,28,29] due to its biocompatibility, high rate of gelation, availability, and ability to be chemically modified for

biomedical applications [30,31]. As such, sodium alginate is used as a model hydrogel herein. Alginate primarily consists of a family of unbranched binary copolymers of 1,4 linked β-D-mannuronic acid (M blocks) and α-L-guluronic acid (G blocks). It undergoes gelation in the presence of divalent ions, such as Ca^{2+}, as the cations take part in the interchain ionic bonding between G-blocks in the polymer chain, which produces a mechanically stable calcium alginate hydrogel. Sodium alginate (Sigma-Aldrich, St. Louis, MO) solutions with final concentrations typical for bioprinting processes including inkjet printing [3,5] and casting (1% w/v) and extrusion printing (4% w/v) were prepared by fully dissolving powder in deionized (DI) water under gentle stirring. Alginate gelation was induced by exposure to a 2% (w/v) calcium chloride ($CaCl_2$) (Sigma-Aldrich, St. Louis, MO) solution prepared by fully dissolving powder in DI water under gentle stirring.

To provide a random high-contrast pattern within the transparent alginate for DIC, white polystyrene beads (Polysciences Inc., Warrington, PA) with a 15 μm diameter were suspended in the respective sodium alginate solutions to a final concentration of 2.5×10^6 beads/mL prior to printing. The final volume fraction represented by the beads was 0.44%, at which the effect on material behavior is assumed to be negligible [32]. While test samples were comprised of alginate herein, the testing and evaluation principles presented are applicable to various hydrogel materials.

2.2. Sample preparation

2.2.1. Fabrication of inkjet-printed samples

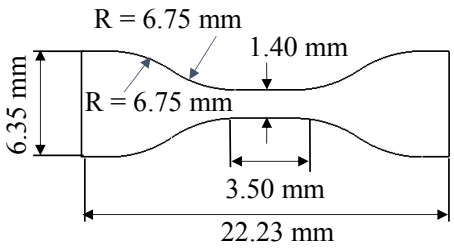

Fig. 1. Designed dimensions for tensile testing samples.

Inkjet printing was used to fabricate 3D samples for DIC under uniaxial tensile testing. The designed "dog bone" geometry utilized herein, shown in Fig. 1, was optimized to ensure failure occurs within the gauge length [26] and was scaled by 75% to be accommodated by the testing apparatus utilized herein. A similar geometry scaled to 80% of the original dimensions has previously been determined by others to be sufficient for mechanical property testing of soft tissue materials [22]. Using a typical inkjet bioprinting approach [3,5], droplets of sodium alginate were deposited onto a substrate to form designed layer shapes which were submerged into a calcium chloride bath to facilitate crosslinking as illustrated in Fig. 2. The movement of a piezoelectric printhead with a 120 μm orifice diameter (Microfab Technologies, Plano, TX) was controlled by a set of motorized linear XY stages (Aerotech, Pittsburgh, PA) [5]. A motorized linear Z stage (Aerotech, Pittsburgh, PA) lowered the printing substrate into the crosslinking bath by the designed layer thickness after each layer was printed. This process continued until complete structures were fabricated layer by layer. The printhead was driven by a bipolar waveform with a ±80 V voltage, 3 μs rise and fall times, and 45 μs dwell and echo times at a frequency of 60 Hz via a JetDrive III controller (MicroFab, Plano, TX).

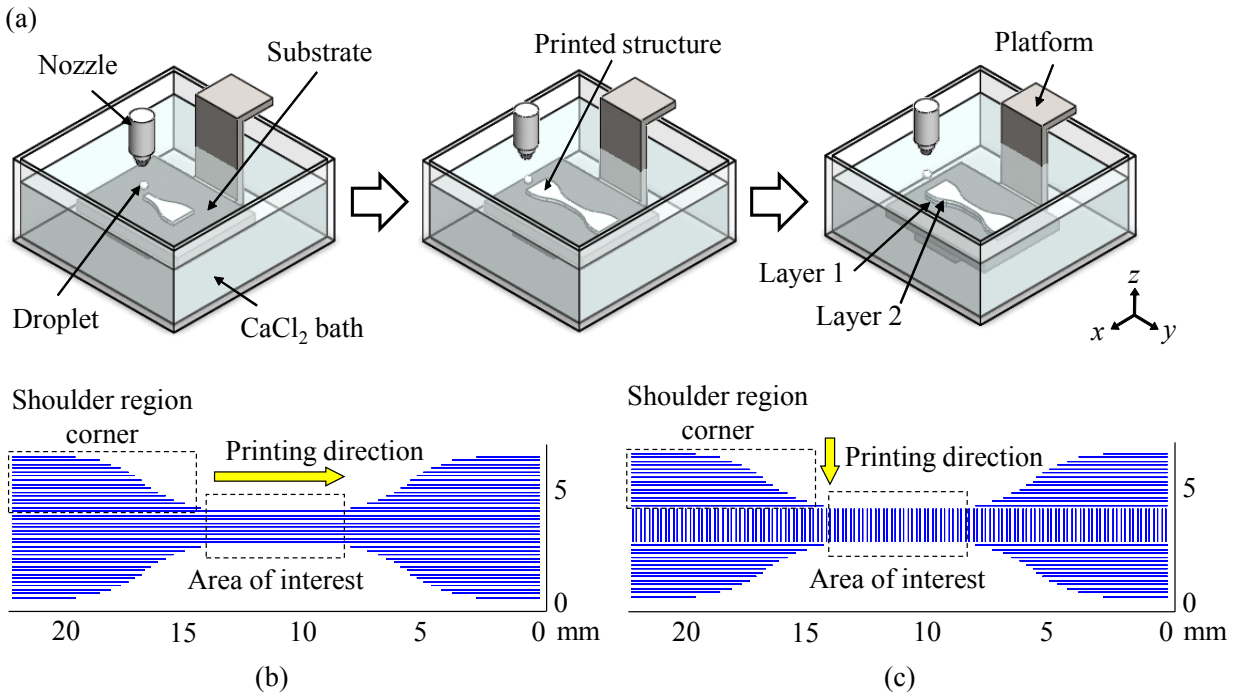

Fig. 2. (a) Inkjet printing approach used for the fabrication of dog bone samples, and design of printed lines for the (b) longitudinal and (c) transverse orientations.

Each printed layer was comprised of a series of adjacent printed lines as shown in Fig. 2(b) and (c), and each plotted line represents a printed line. Depending on printing conditions and printing path orientation, interfaces may form between adjacent lines within inkjet-printed layers [25]. Two printing path configurations were investigated herein, longitudinal (Fig. 2(b)) and transverse (Fig. 2(c)), which aimed to identify the effects of interface orientation on the strain distribution for samples under uniaxial tension. The four corners of the shoulder regions for both longitudinal (Fig. 2(b)) and transverse (Fig. 2(c)) samples were printed longitudinally to improve consistency between samples as well as for programming convenience. To achieve a thickness adequate for handling during testing, each sample consisted of five printed layers, each with identical XY printing paths and a thickness of 50 μm, to achieve a final sample thickness of

250 μm. The effects of interfaces between subsequently printed layers are assumed to be negligible compared to interfaces between adjacent lines within layers due to the direction of loading during uniaxial tensile testing. A spacing of 140 μm between adjacent printed lines and a nozzle travel speed of 3.33 mm/s led to well-defined layers. For each printing path orientation, parameters including droplet deposition frequency, printing velocity, and distance between printed lines were held constant in order to investigate the effects of printing path orientation for a given set of printing parameters. Due to the spread of material during printing and hydrogel swelling, samples were found to have dimensions slightly larger than designed, which were accounted for in subsequent calculations. After printing, samples were submerged in a 2% calcium chloride bath for 1 hour for further gelation before testing.

2.2.2. Fabrication of cast control samples

Casting was used to produce homogeneous samples which lack interfaces for a mechanical property benchmark comparison. A custom Sylgard 184 polydimethylsiloxane (PDMS) (Dow Corning, Auburn, MI) mold was created with the designed "dog bone" geometry (Fig. 1) and a sample thickness of 250 μm. Sodium alginate was added dropwise to fill the mold and a layer of foam was placed on top. Then, 2% calcium chloride solution was added dropwise to saturate the layer of foam and facilitate alginate gelation. After an initial gelation period of 60 seconds to increase the robustness of the alginate sample, the mold was submerged in a 2% calcium chloride solution for 1 hour for further gelation.

2.2.3. Fabrication of extrusion-printed control samples

Samples were prepared by extrusion printing to act as a control which has defined interfaces as shown in Fig. 3. Rather than printing discrete samples, 30 × 30 mm testing sheets

printed as a series of adjacent parallel lines were fabricated using a serpentine printing path and cut into rectangular samples. Samples were cut from the edge of printed sheets such that visible interfaces existed between alternating pairs of adjacent lines. That is, coalescence was prevented and an interface was formed between adjacent lines for which the feed between lines was at the opposite end of the printed sheet, as has been observed during inkjet printing [25]. The orientation of printed lines and resulting interfaces was analogous to the transverse orientation used for inkjet-printed samples. Sheets were fabricated using an nScrypt 3Dn-450-HP (nScrypt, Orlando, FL) extrusion system as described in previous studies [9,10]. Continuous filaments were deposited onto a foam substrate saturated with 2% calcium chloride by a 200 μm diameter nozzle with an applied pressure of 103 kPa (15 psi) and a nozzle travel speed of 1 mm/s. As observed, some regions between each printed filament were gelled before adjacent material was deposited such that coalescence was prevented and an interface was formed. Since extrusion printing is capable of fabricating thick layers by using a large diameter nozzle, testing sheets were printed as a single layer with a thickness of approximately 200 μm. Following deposition, the sheets were immediately transferred to a bath of 2% calcium chloride to facilitate further crosslinking for 1 hour. Immediately before testing, 5×15 mm rectangular samples were manually cut using a lab scalpel.

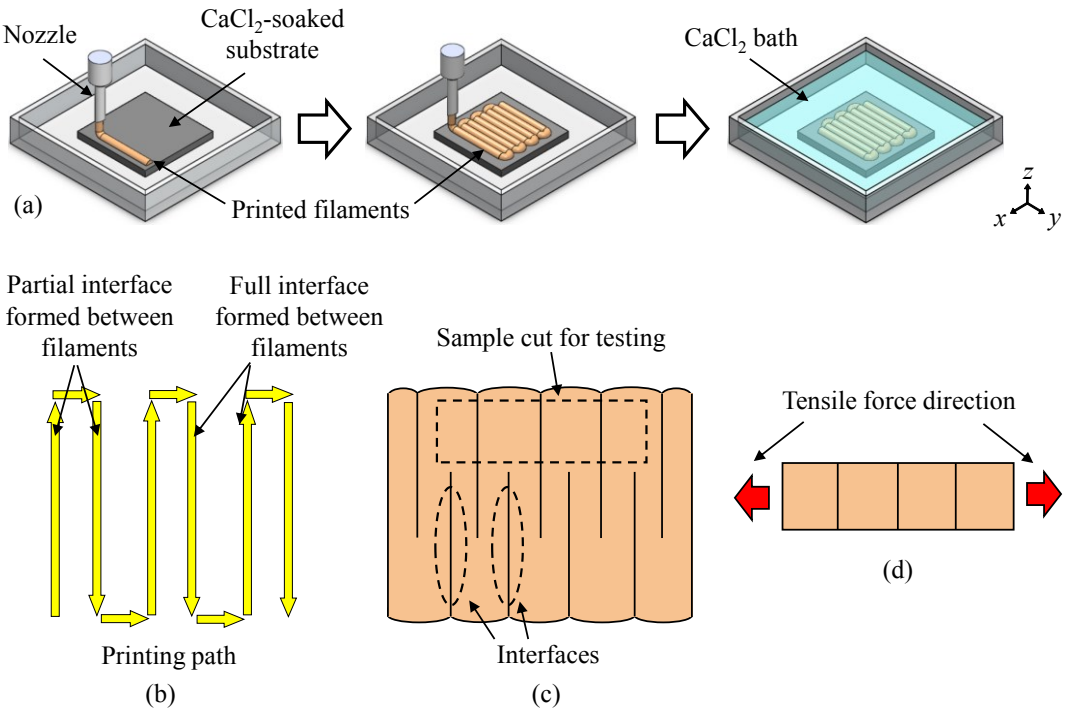

Fig. 3. (a) Extrusion printing approach used for the fabrication of testing sheets, (b) serpentine printing path design for filament deposition, (c) representation of a resulting sheet with interfaces between alternating pairs of lines, and (d) representation of a cut sample with interfaces.

2.3. Digital image correlation and tensile testing

The effects of interfaces and their orientation on local strain distributions within printed samples under uniaxial tension were investigated using DIC. Herein, an eXpert 4000 Micro Tester (ADMET, Norwood, MA) micromechanical tensile testing system equipped with compression grips and a 50 g load cell was used to introduce uniaxial tension to samples, and DIC was conducted to quantify variations in local strain due to the effects of interfaces. Testing times were relatively short compared to the rate of evaporation and testing began immediately after removal of samples from their respective crosslinking baths, such that the effects of drying

are assumed to be negligible. While not the primary focus herein, load and displacement data were recorded during tensile testing to offer insight into the effects of interfaces on mechanical properties including the effective stiffness (analogous to the Young's modulus at high strains), failure strength, and failure strain. Unlike other mechanical testing approaches, such as compression or needle insertion, tensile testing offers the ability to orient tensile forces parallel or perpendicular to interfaces formed between adjacent lines within a printed layer.

The tensile testing system was mounted on an inverted microscope (EVOS, Thermo Fisher Scientific, Waltham, MA), which was used for DIC-related imaging as shown in Fig. 4. One grip remained stationary while the other translated with a cross-head speed of 0.015 mm/s to ensure that the deformation between subsequent images used for DIC was sufficiently small. The maximum crosshead displacement observed during DIC experiments was approximately 2 mm due to the field of view of the microscope system, limiting the strain of samples to a maximum of approximately 0.40. The microscope was used to digitally acquire a reference image of the testing region before loading as well as images of the deformed gage section during loading at 10 second intervals until sample failure. Load-displacement data was simultaneously recorded by the tensile testing system. After testing was complete, images were analyzed using the DaVis DIC software (LaVision, Göttingen, Germany), which output the displacement, velocity, and strain distribution within the testing section. For this correlation, a subset and step size of 51×51 and 4 pixels were used, respectively. A curvilinear 90% decay filter with a filter size of 15 pixels was used to average and smooth the extracted strain data.

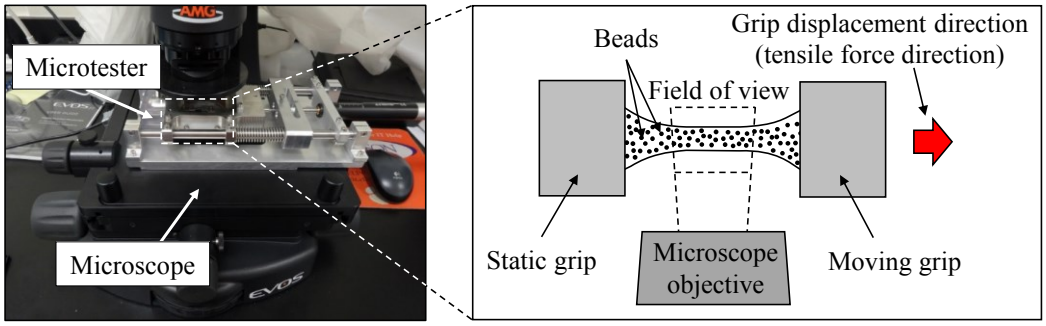

Fig. 4. Schematic showing the placement of the microtester and sample in the EVOS microscope

3. Interface formation during inkjet printing

During inkjet and other droplet-based printing, a printed layer may consist of a series of parallel printed lines with short feed distances between lines. Under ideal inkjet printing conditions, the rapid deposition of droplets enables the fabrication of continuous lines without interfaces between droplets [25]. However, interfaces may form between two adjacent lines depending on the state of gelation of adjacent regions [25]. That is, if the material from a previously printed line remains a fluid when adjacent new material is deposited, the printed regions coalesce and an interface does not form. Conversely, if the material from a previously printed line is already solidified when adjacent new material is deposited, coalescence can be prevented and an interface may form.

During the fabrication of layers as illustrated in Fig 5. (a) and (b), gelation of printed material begins to occur immediately after deposition because of ion diffusion through the previously printed layer onto which each new layer is deposited. Partial coalescence (Fig. 5 (c)) may occur for adjacent regions in which the previously printed material is gelled partially through its thickness, due to the time required for full-thickness gelation of a printed line,

whereas no coalescence occurs and a full interface is formed (Fig. 5 (d)) between adjacent regions if the previously printed material is gelled through its full thickness. Both partial and full interfaces may affect the mechanical behavior of printed layers. Specifically, interfaces may lead to localized regions of excessive deformation for samples under uniaxial tension when the loading acts to pull apart adjacent printed lines.

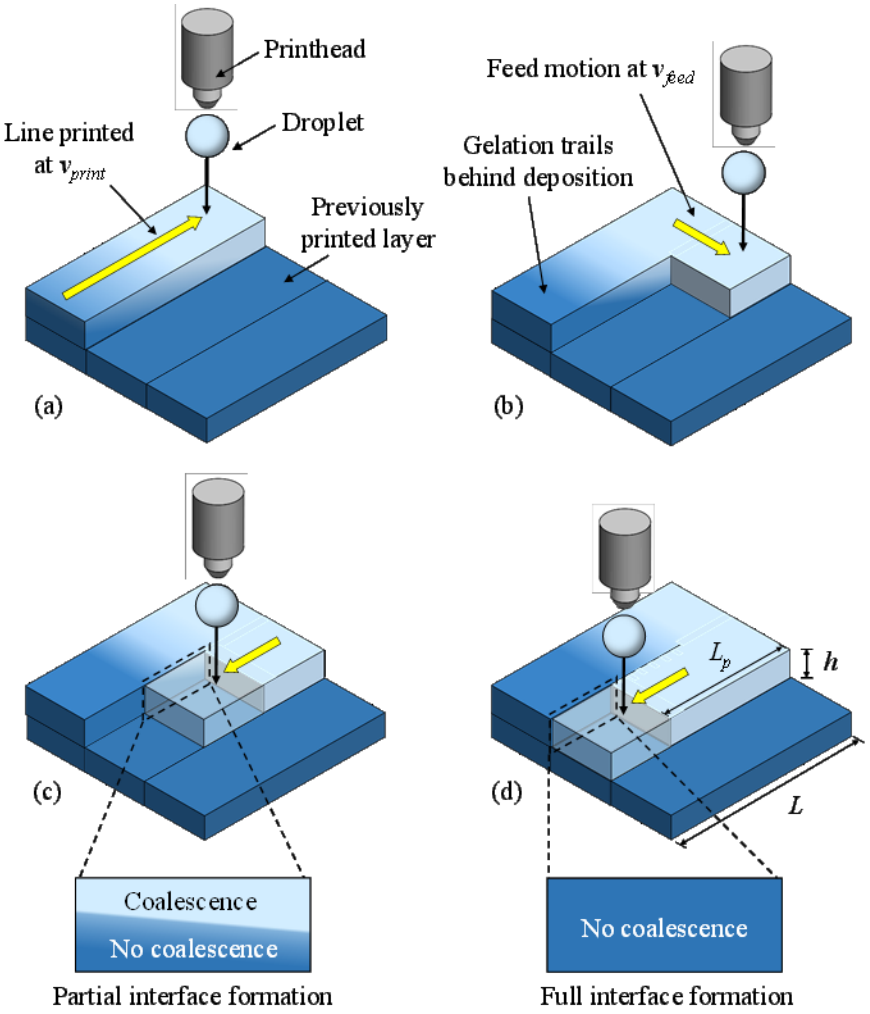

Fig. 5. (a)-(d) Illustration of the formation process of partial and full interfaces between two adjacent printed lines depending on the gelation state of the first printed line. Darker regions indicate gelled material and lighter regions indicate fluidic material.

The gelation state of a printed line may be predicted based on a reaction-diffusion model in which a gelation front travels through the thickness of a printed layer [7,25,33]. For sodium alginate being crosslinked by calcium chloride, rearranging terms and assuming a filter length of zero [25,33] yields the time (Δt_{full}) required for the full thickness of a printed line or layer to be gelled as shown in Equation (1):

$$\Delta t_{full} = \frac{h^2}{2D_C\theta} \tag{1}$$

where h is the layer thickness, D_c is the diffusion coefficient of free calcium ions, shorthand notation of the calcium cation bulk concentration is defined as $\theta = \frac{C_0}{N_c a_0}$ [33], C_0 is the calcium cation bulk concentration, a_0 is the bulk concentration of printed alginate solution, and $N_c = \frac{3}{4}G$ is the stoichiometric calcium cation binding capacity [34] for alginate solutions with guluronic acid content G.

Full interface formation occurs when adjacent regions are deposited next to a line which has already gelled through its full thickness as predicted by Equation (1). From this, the length of partial interface formation L_p between two adjacent lines measured from the feed between the lines (Fig. 5(b)) can be predicted by Equation (2) based on Δt_{full}, v_{print} (printhead travel speed during printing), d_{feed} (feed distance), and v_{feed} (printhead feed speed):

$$L_p = \frac{v_{print}}{2}\left(\Delta t_{full} - \frac{d_{feed}}{v_{feed}}\right) \tag{2}$$

Solving Equation (2) for the gelled thickness through the layer height h and integrating over L_p gives the interfacial area within the region of partial interface formation. Accounting for the interfacial area within the region of full interface formation, the interface fraction (*IF*), representing the ratio of interfacial area to the total contact area between two adjacent printed

lines in direct contact with each other, can then be expressed as Equation (3) for adjacent lines of a total length of L as shown in Fig. 5:

$$IF = 1 - \frac{v_{print}}{2L}\left(\frac{\Delta t_{full}}{3} - \frac{d_{feed}}{v_{feed}}\right) \tag{3}$$

Equation (3) is based on the material deposition rate compared to that of gelation such that it may be applicable to various printing approaches in addition to inkjetting. The *IF* for a given set of printing conditions offers insight into the degree of interface formation and may be used to gauge the interface effects on mechanical behavior. When the deposition rate of two adjacent lines is higher than the rate of gelation, the majority of the two lines coalesces as a liquid before gelation and the *IF* may be near 0. Conversely, if the deposition rate of two adjacent lines is small compared to the rate of gelation, the majority of the two lines does not coalesce and the *IF* may be near 1.

4. Experimental Results on Effects of Interfaces on Local Strain Distributions

In this study, local strain is displayed as a heat map as indicated by the displayed scale where the red color indicates regions of relatively large deformation and the blue color represents regions of relatively small deformation. The sequence of images (a)-(e) of Figs. 8-10 were acquired at axial strains of 0.05, 0.15, 0.25, 0.35, and 0.45, respectively, based on the grip displacement during testing.

4.1. Inkjet printed parts

For inkjet-printed samples with the transverse orientation fabricated herein, the rate of deposition of adjacent lines compared to the rate of gelation is such that regions of both partial and full interfaces exist. Equation (1) predicts Δt_{full} is 0.63 s for a typical scenario when h = 50

μm, D_c = 0.77×10^{-9} m^2 s^{-1} [35], C_0 = 0.136 mol L^{-1}, a_0 = 0.1 mol L^{-1}, and G = 0.7 [36]. The minimum time between adjacent regions being deposited, Δt_{min}, in the testing width for the transverse orientation is 0.014 s and the maximum time, Δt_{max}, is 0.77 s since d_{feed} is 140 μm, v_{feed} is 10 mm/s, W (testing region width) is 1.40 mm as shown in Fig. 1, which was achieved due to material spreading when using a print path length of 1.26 mm, and v_{print} is 3.33 mm/s. This indicates that some coalescence will occur as Δt_{min} is less than Δt_{full}, but a full interface will also be formed in some regions as Δt_{max} is larger than Δt_{full}. Equation (2) predicts that the length of partial interface formation L_p is 1.02 mm such that for the sample width of 1.40 mm, a full interface exists across 0.38 mm of the width. Equation (3) predicts that the interface fraction IF is 0.77, indicating that 77% of the area between two adjacent printed lines does not coalesce and is instead an interface. Such interfaces may significantly affect the mechanical behavior of inkjetting samples printed with the transverse printing path.

Regions of coalescence and interface formation are further predicted for adjacent lines within the transverse inkjet-printed sample by considering the gelation front location during deposition. As shown in Fig. 6, the location of the gelation front at the time adjacent material is deposited can be determined by the reaction-diffusion model [7,25,33]. The curve delineates the coalescence status at any location along a printing path as two scenarios: for the partial interface scenario, coalescence (no interface) occurs above this curve and no coalescence (interface) occurs beneath this curve; for the complete interface scenario, no coalescence occurs through the layer thickness.

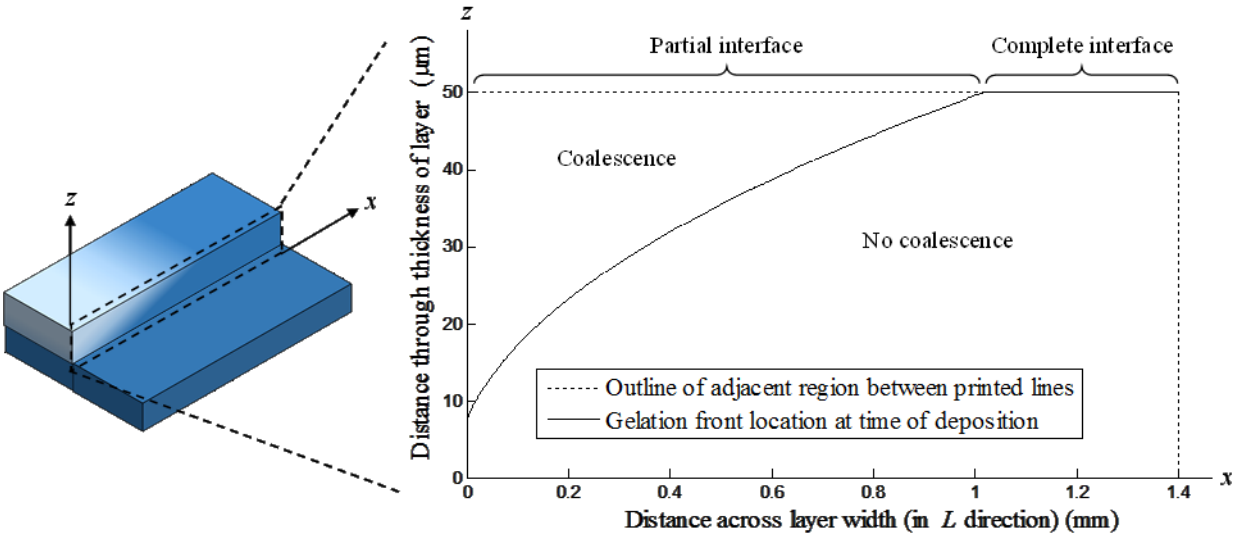

Fig. 6. Plot of gelation front location through the thickness of a printed layer at the time of adjacent material deposition during alginate printing for h = 50 μm, W = 1.40 mm, d_{feed} = 140 μm, v_{feed} = 10 mm/s, and v_{print} = 3.33 mm/s. Fluid material above the gelation front coalesces while material below the gelation front forms an interface.

For samples printed with the longitudinal orientation, Δt_{min} in the testing width is 5.63 s and Δt_{max} is 7.90 s due to the long travel distance between adjacent lines (9.37 mm at the shortest) along the printing path. Since both of them are longer than the predicted Δt_{full} of 0.63 s, coalescence does not occur along the entire adjacent region between two lines and a full interface is formed. As such, the longitudinal orientation printing results in an *IF* of 1.

Samples fabricated using conditions identical to the samples used for testing are shown in Fig. 7, and there are no polystyrene beads included in order to improve clarity. Samples printed with the longitudinal orientation exhibit defined interfaces along the length of the testing section as shown in Fig. 7 (a). Due to the large time between the deposition of adjacent material for the longitudinal orientation, no coalescence is observed and full interfaces are formed. Samples

printed with the transverse orientation show apparent but poorly defined interfaces along the width of the testing section as shown in Fig. 7 (b), indicative of the formation of partial interfaces between the lines. Some undesirable material buildup is visible along the transverse sample edges due to frequent high speed feeds between the printed lines, but the effect of this region is assumed negligible during testing.

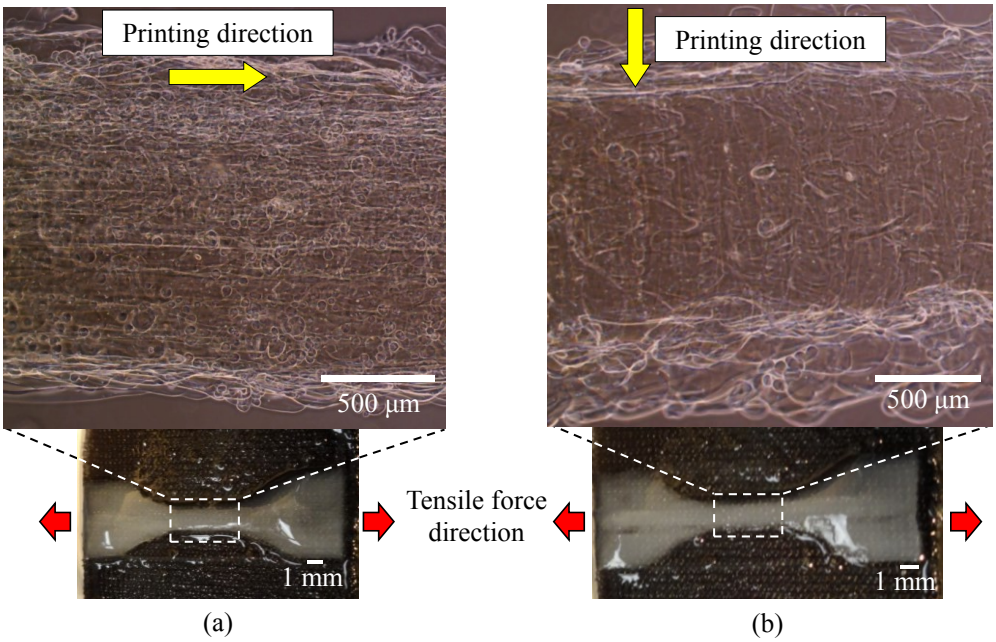

Fig. 7. Printed samples exhibiting visible interfaces between printed lines for (a) longitudinal and (b) transverse printing path orientations.

Strain analysis using DIC for an inkjet-printed sample with the transverse orientation during tensile testing is shown in Fig. 8, and Fig. 8(a) also illustrates some locations of interfaces between printed lines. As seen from Fig. 8, there is no observable localized regions of increased strain under uniaxial tension, indicating that strain distributions are homogeneous throughout the

sample despite the presence of partial and full interfaces between adjacent lines within layers. Since regions of increased strain are not visible along interfacial regions between adjacent lines as would occur due to delamination or decreased bonding strength between printed lines, there is no pronounced effect of interfaces on local deformation. Minor local strain concentrations are attributed to imperfections in surface texture, bead distribution, and strain analysis. Similarly, DIC analysis of samples with the longitudinal orientation yields identical results such that they are not included herein. While increased localized strain may be expected along interfaces for inkjet-printed samples, this is not observed as can be seen in Fig. 8. This is attributed to the multi-layer nature of the inkjet-printed samples, and will be discussed in details later.

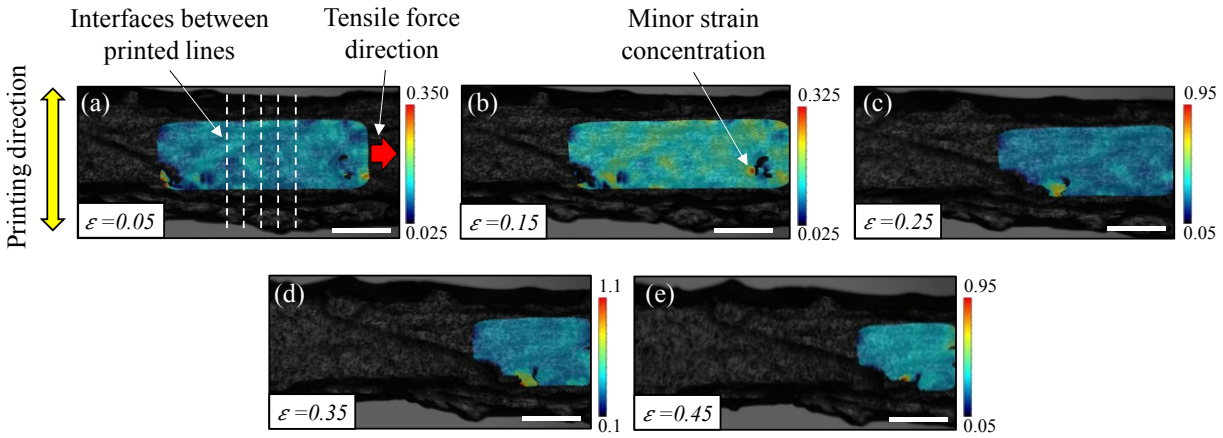

Fig. 8. (a)-(e) Strain distributions using DIC for an inkjet-printed sample with the transverse printing path orientation under uniaxial tension at axial strains of 0.05, 0.15, 0.25, 0.35, and 0.45, respectively (scale bars = 500 μm). No correlation is found for small black regions within the strain data due to sample imperfections.

4.2. Cast parts

As expected for homogeneous materials, cast samples exhibit homogeneous strain distributions under uniaxial tension. Strain analysis using DIC for a cast sample during tensile testing is shown in Fig. 9. By inspection, strain distributions across cast samples are more uniform than for inkjet-printed samples due to fewer imperfections in surface texture and bead distribution. Minor local strain concentrations are attributed to sample and testing imperfections.

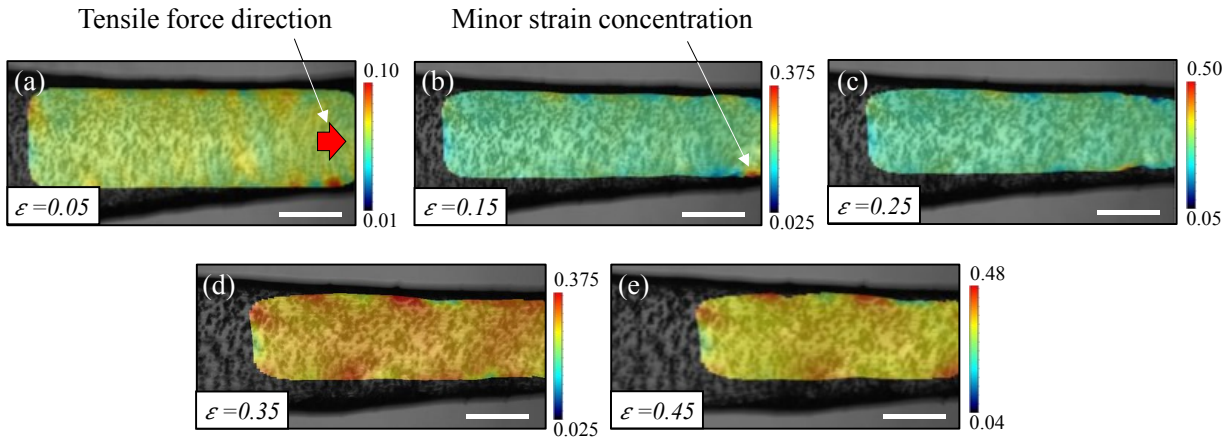

Fig. 9. (a)-(e) Strain distributions using DIC for a homogeneous cast sample under uniaxial tension at axial strains of 0.05, 0.15, 0.25, 0.35, and 0.45, respectively (scale bars = 500 μm).

4.3. Extrusion printed part

Like inkjet printing, the possibility of forming interfaces using extrusion printing depends on the time between adjacent filaments being printed and the time for the full gelation of printed lines. Equation (1) predicts that the time (Δt_{full}) required for the full thickness of each printed line to be solidified is 20.1 s for a layer thickness h of 200 μm during extrusion for which the bulk concentration of printed alginate solution a_0 is 0.2 mol L^{-1}, or twice that of the alginate solution

used for inkjet printing. The increased layer thickness and alginate concentration when compared to the inkjet-printed samples leads a substantially larger Δt_{full} for extrusion-printed samples (20.1 s vs. 0.63 s). Despite the increased gelation time during extrusion, full interfaces are formed during the fabrication of sheets (Fig. 3) due to the increased total length L and decreased v_{print} of 1 mm/s compared to inkjet printing. The feed distance d_{feed} and printhead feed speed v_{feed} during extrusion printing were identical to those of inkjet printing. For a sheet with a 30 mm width, Equation (2) predicts the length of partial interface formation L_p as 10.0 mm, resulting in a full interface across the remaining 20 mm sheet width. This indicates that adjacent filaments alternate between forming full interfaces (feed between filaments is at the opposite end of sheet) and partial interfaces (feed between filaments at the same end of the sheet from which the testing sample is cut) as illustrated in Fig. 3(b). The interface fraction IF is 1 for full interfaces, and Equation (3) predicts IF as 0.33 between filaments which partially coalesce along the 5 mm width of the 5×15 mm rectangular testing samples.

Fig. 10 illustrates the strain analysis results using DIC for an extrusion-printed sample with a printing path orientation analogous to the transverse inkjet-printed samples, such that tensile force acts to pull apart adjacent regions at interfaces between printed lines, during tensile testing. Unlike the inkjet-printed and cast samples, localized regions of increased strain are observed as evenly spaced vertical bands as indicated by orange/red regions of high deformation relative to blue/green regions of low deformation. The distance between the vertical bands of increased strain corresponds with the distance between alternating pairs of adjacent lines, or twice the printed line width, and indicates that increased strain occurs at the interfaces between filaments. Strain within each printed line and between coalesced lines is largely uniform, with small variations being attributed to sample imperfections. Unlike inkjet-printed and cast samples

which both exhibit a homogeneous strain distribution, extrusion-printed samples clearly exhibit anisotropic behavior under tension due to the effects of interfaces between printed lines.

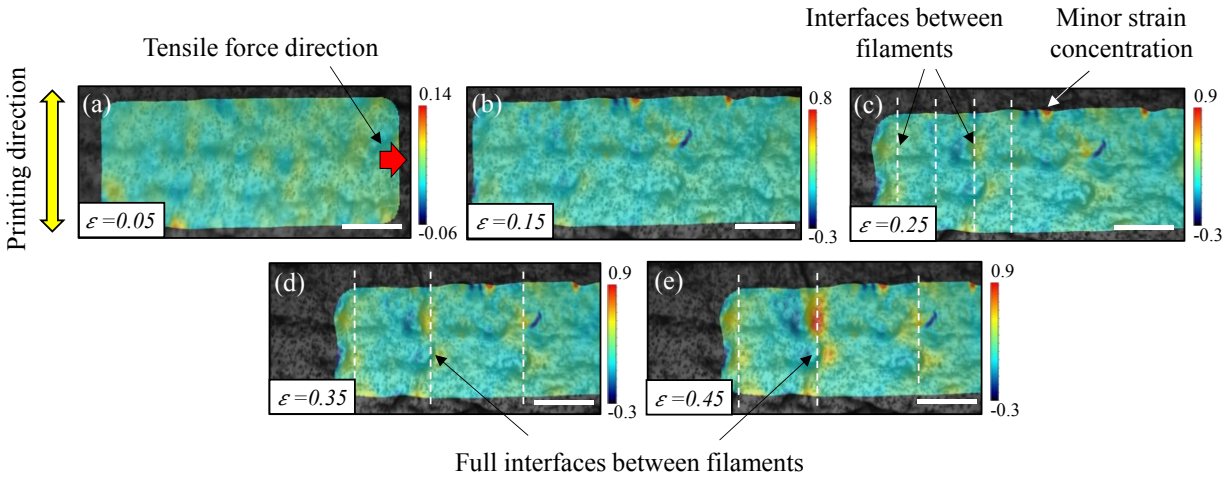

Fig. 10. (a)-(e) Strain distributions using DIC for an extrusion-printed sample with the transverse printing path orientation under uniaxial tension at axial strains of 0.05, 0.15, 0.25, 0.35, and 0.45, respectively (scale bars = 500 μm).

5. Discussion

5.1. Visualization of local strains

For the formation of interfaces, newly deposited material may bond more weakly with the already solidified region when compared to those coalesced without an interface since most bonding sites within a gelled layer are already occupied by calcium cations. Interfacial regions of samples prepared by both inkjet and extrusion printing may display regions of increased local strains under uniaxial tension due to this decreased bond strength. In particular, samples with a

transverse printing path orientation (Fig. 11(a)), in which tensile forces pull apart printed lines, may experience increased local deformation along interfacial features.

While local deformation is observed for the extrusion-printed samples as shown in Fig. 10, a homogeneous strain distribution is observed for the inkjet-printed samples as shown in Fig. 8. As predicted using Equations (1) and (2), interfaces exist within the inkjet-printed samples tested herein. The lack of pronounced localized regions of increased strain may be attributed to the samples being printed in 5 layers in this study, whereas extrusion-printed samples were printed as a single-layer sheet. As illustrated in Fig. 11(b), the locations of interfaces within each layer of the five-layer inkjet-printed samples may not be consistent. As a result, there is no well-defined interface region within the inkjet-printed samples due to the inconsistency of the interfaces across different layers. Without a well-defined interfacial region throughout the full sample thickness, defined regions of increased local strain cannot be adequately visualized using DIC. Despite the inability to visualize their effects using DIC, interfaces within each printed layer may still affect the mechanical properties of printed structures. Ideally, single-layer inkjet-printed samples with defined interfacial regions would be tested, but single-layer sheets lack the mechanical robustness required for handling during testing.

Additionally, as predicted, the samples fabricated by inkjet printing have substantial regions of partial interface formation while the samples from extrusion printing have regions of full interface formation across the testing width. Generally, increased local strains are not observed along partial interfaces for the inkjet-printed or extrusion-printed samples. Compared to partial interfaces, full interfaces may have a more pronounced effect on local strain distributions, such that they may be more readily visualized using DIC as shown in Fig. 10.

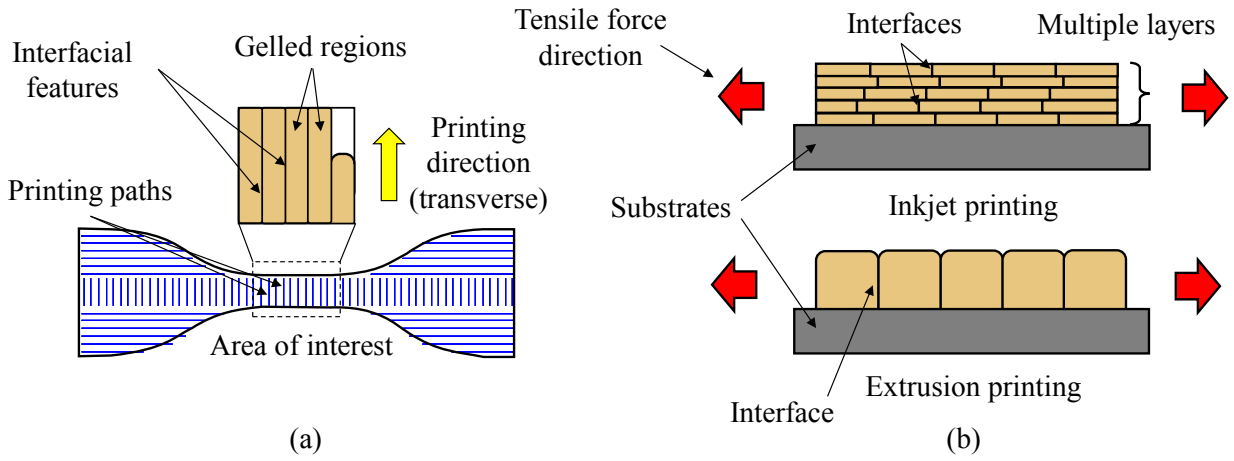

Fig. 11. (a) Top and (b) side views of samples with transverse printing path orientations fabricated by inkjet and extrusion printing, illustrating potential misalignment of interfaces for the inkjet-printed samples.

5.2. Effects on mechanical properties

While not the primary focus herein, the load and displacement data were recorded during tensile testing of the inkjet-printed 1% alginate samples to offer insight into the effects of interfaces on mechanical properties including the effective stiffness (E), failure strength, and failure strain ($\varepsilon_{failure}$). Representative stress-strain curves of the longitudinally and transversely inkjet-printed samples and cast samples are shown in Fig. 12. The general shape of the stress-strain curves are in good agreement with those of soft materials during tensile testing [12]. A linear region is evident regardless of the fabrication method and is used to determine the effective stiffness, analogous to the Young's modulus at high strains, of the material. The failure strength and failure strain are also determined from the stress-strain curve when the stress and strain reach their maximums, respectively.

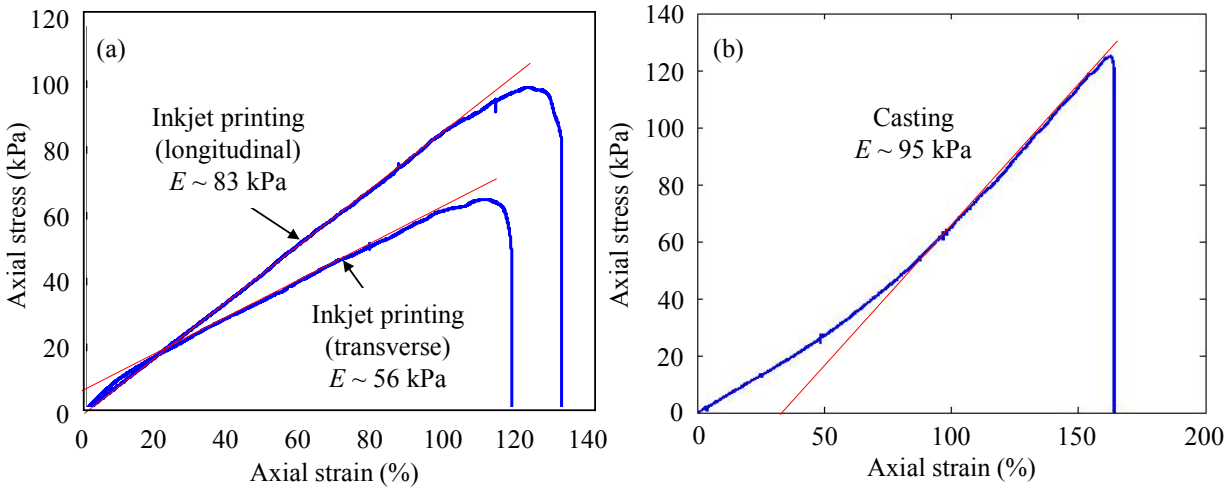

Fig. 12. Representative stress-strain curves for (a) inkjet-printed samples with longitudinal and transverse printing orientations and (b) cast sample.

While the overall trend is consistent across several samples, the magnitudes of mechanical properties were found to vary due to inconsistencies in the fabrication process. For illustration, only results from a single set of three samples for which the effective stiffness and failure strength are on the order of reported values for alginate gels [9,17,37] are included herein. Table 1 shows the mechanical properties for the representative inkjet-printed samples with the transverse and longitudinal printing path orientations and the cast samples, and there is a strong dependency of the mechanical properties on the printing path orientation. For the transversely printed samples, printed lines are perpendicular to the axial loading direction, such that delamination occurs and the effects on the mechanical properties are pronounced. Significant decreases in the effective stiffness, failure strength, and failure strain may be attributed to the decreased bond strength at interfaces between printed lines. Longitudinally printed samples also exhibit a decrease in the effective stiffness, failure strength, and failure strain when compared to

the cast samples, but to a lesser extent. While the effects of interfaces on local strains observed using DIC are not pronounced herein, interfaces with the transverse orientation have a more pronounced effect on mechanical properties when compared to the longitudinal orientation, illustrating the significance of printing path orientation.

Table 1 Mechanical properties of 1% (w/v) sodium alginate samples

Fabrication method	E (kPa)	Failure strength (kPa)	$\varepsilon_{failure}$ (%)
Transverse inkjet printing	56	67	112
Longitudinal inkjet printing	83	100	124
Casting	95	125	158

6. Conclusions

The mechanical deformation of 3D printed alginate structures was quantified using digital image correlation (DIC) and uniaxial tensile testing. Inkjet and extrusion printing were used to fabricate testing samples with interfaces between adjacent lines, and casting was used to create homogeneous samples. In particular, the effects of interfaces between printed lines within a layer on strain distributions were investigated using DIC. The formation of partial and full interfaces was discussed, and the prediction of the ratio of interfacial area to the total contact area between two adjacent printed lines was presented as a function of printing conditions and gelation parameters.

Some main conclusions are drawn as follows. First, despite the formation of interfaces between adjacent lines, inkjet-printed samples with both longitudinal and transverse printing path orientations exhibit uniform strain distributions under uniaxial tension. The inability to observe defined regions of increased strain between printed lines using DIC may be attributed to the multi-layer nature of inkjet-printed samples which lack defined regions of full interface formation. Second, despite the inability to observe the effects of interfaces, printing path orientation (and resulting interface orientation) is found to have a significant effect on the effective stiffness, failure strength, and failure strain of inkjet-printed samples. In particular, samples with the transverse printing path orientation exhibit a substantial decrease in these properties when compared to homogeneous cast samples, which may be attributed to delamination between printed lines and reduced bond strength at interfaces. Samples with the longitudinal printing path orientation also exhibit a decrease in these properties compared to cast samples, but to a much lesser extent. Finally, unlike inkjet-printed samples, extrusion-printed samples (single layer) exhibit defined regions of increased deformation and anisotropic behavior under tension. The distance between localized bands of increased strain corresponds with the distance between alternating pairs of adjacent lines as extruded, indicating that increased strain occurs at full interfaces between filaments.

Therefore, printing path design, printing conditions, and gelation conditions have been shown to affect the deformation behavior and resulting properties of printed structures. In particular, resulting interfaces may lead to regions of increased localized deformation and significant decreases in mechanical properties. Thus, print path design, printing conditions, and gelation parameters should be optimized when fabricating hydrogel structures. For uniform deformation and improved mechanical properties of printed structures, the time between the

deposition of adjacent regions should be controlled such that the formation of interfaces is minimized. If interface formation cannot be minimized, printing paths should be designed such that the direction of expected loading is not perpendicular to resulting interfaces in order to reduce the effects of delamination. This study represents the first step toward describing the deformation and mechanical behavior of hydrogel structures both quantitatively and qualitatively, and future work may aim to further develop the presented methods for improved accuracy. Strain distributions and mechanical properties within single-layer inkjet-printed samples with full interfaces rather than partial interfaces should be investigated and the significance of the interface fraction on resulting mechanical properties should be experimentally validated. Additionally, future work may include similar investigation of interfaces formed between subsequently printed layers in the build direction and further microstructural characterization, including experimental validation of the predicted interface fraction.

Acknowledgements:

This work is partially supported by the US National Science Foundation (CMMI-1634755). The experimental contributions from Sijia Lyu and Pei-Ying Wu and the discussion with Dr. Yong He are highly appreciated.

References:

[1] B.R. Ringeisen, R.K. Pirlo, P.K. Wu, T. Boland, Y. Huang, W. Sun, Q. Hamid, D.B. Chrisey, cell and organ printing turns 15: diverse research to commercial transitions, MRS Bull. 38(10) (2013) 834-843.

[2] Y. Huang, M.C. Leu, J. Mazumder, A. Donmez, Additive manufacturing: current state, future potential, gaps and needs, and recommendations, J. Manuf. Sci. Eng. 137(1) (2015) 014001.

[3] C. Xu, W. Chai, Y. Huang, R.R. Markwald, Scaffold-free inkjet printing of three-dimensional zigzag cellular tubes, Biotechnol. Bioeng. 109(12) (2012) 3152-3160.

[4] C. Xu, Z. Zhang, K. Christensen, Y. Huang, J. Fu, R.R. Markwald, Freeform vertical and horizontal fabrication of alginate-based vascular-like tubular constructs using inkjetting, J. Manuf. Sci. Eng. 136(6) (2014) 061020.

[5] K. Christensen, C. Xu., W. Chai, Z. Zhang, J. Fu, Y. Huang, Freeform inkjet printing of cellular structures with bifurcations, Biotechnol. Bioeng. 112(5) (2014) 1-10.

[6] B.C. Riggs, A.D. Dias, N.R. Schiele, R. Cristescu, Y. Huang, D.T. Corr, D.B. Chrisey, Matrix-assisted pulsed laser methods for biofabrication, MRS Bull. 36(12) (2011) 1043–1050.

[7] R. Xiong, Z. Zhang, W. Chai, Y. Huang, D.B. Chrisey, Freeform drop-on-demand laser printing of 3D alginate and cellular constructs, Biofabrication 7(4) (2015) 045011.

[8] A. Skardal, J. Zhang, G. Prestwich, Bioprinting vessel-like constructs using hyaluronan hydrogels crosslinked with tetrahedral polyethylene glycol tetracrylates, Biomaterials 31 (2010) 6173–6181.

[9] Y. Jin, A. Compaan, T. Bhattacharjee, Y. Huang, Granular gel support-enabled extrusion of three-dimensional alginate and cellular structures, Biofabrication 8(2) (2016) 025016.

[10] Y. Jin, A. Compaan, W. Chai, Y. Huang, Functional nanoclay suspension for printing-then-solidification of liquid materials, ACS Appl. Mater. Interfaces 9(23) (2017) 20057-20066.

[11] Y. Jin, W. Chai, Y. Huang, Printability study of hydrogel solution extrusion in nanoclay yield-stress bath during printing-then-gelation biofabrication, Mater. Sci. Eng. C 80 (2017) 313-325.

[12] J.L. Drury, R.G. Dennis, D.J. Mooney, The tensile properties of alginate hydrogels, Biomaterials 25 (2004) 3187-3199.

[13] M. Moresi, M. Bruno, Characterization of alginate gels using quasi-static and dynamic methods, J. Food Eng. 82 (2007) 298-309.

[14] T. Becker, D. Kipke, T. Brandon, Calcium alginate gel: a biocompatible and mechanically stable polymer for endovascular embolization, J. Biomed. Mater. Res. 54 (2000) 76-86.

[15] C.K. Kuo, P.X. Ma, Maintaining dimensions and mechanical properties of ionically crosslinked alginate hydrogel scaffolds in vitro, J. Biomed. Mater. Res. 84(4) (2007) 899-907.

[16] L.Q. Wan, J. Jiang, D.E. Arnold, X.E. Guo, H.H. Lu, V.C. Mow, Calcium concentration effects on the mechanical and biochemical properties of chondrocyte-alginate constructs, Cell. Mol. Bioeng. 1(1) (2008) 93-102.

[17] G. Kaklamani, D. Cheneler, L. Grover, M. Adamsa, J. Bowen, Mechanical properties of alginate hydrogels manufactured using external gelation, J. Mech. Behav. Biomed. Mater. 36 (2014) 135-142.

[18] U. Ajoku, N. Saleh, N. Hopkinson, R. Hague, P. Erasenthiran, Investigating mechanical anisotropy and end-of-vector effect in laser-sintered nylon parts, Proc. Inst. Mech. Eng., Part B 220(7) (2006) 1077-1086.

[19] C.S. Lee, S.G. Kim, H.J. Kim, S.H. Ahn, Measurement of anisotropic compressive strength of rapid prototyping parts, J. Mater. Process. Technol. 187 (2007) 627-630.

[20] M.W. Barclift, C.B. Williams, Examining variability in the mechanical properties of parts manufactured via polyjet direct 3D printing, Solid Freeform Fabr. Symp. Proc. August (2012) 6-8.

[21] A. Farzadi, M. Solati-Hashjin, M. Asadi-Eydivand, N.A.A. Osman, 2014. Effect of layer thickness and printing orientation on mechanical properties and dimensional accuracy of 3D printed porous samples for bone tissue engineering, PloS one 9(9) (2014) e108252.

[22] B. Duan, L. Hockaday, K. Kang, J. Butcher, 3D bioprinting of heterogeneous aortic valve conduits with alginate/gelatin hydrogels, J. Biomed. Mater. Res., Part A 101A (5) (2013) 1255-1264.

[23] T.J. Hinton, Q. Jallerat, R.H. Palchesko, J.H. Park, M.S. Grodzicki, J.J. Shue, M.H. Ramadan, A.R. Hudson, A.W. Feinberg, Three-dimensional printing of complex biological structures by freeform reversible embedding of suspended hydrogels, Sci. Adv. 1(9) (2015) 1-10.

[24] A.M. Compaan, K. Christensen, Y. Huang, Inkjet bioprinting of 3D silk fibroin cellular constructs using sacrificial alginate, ACS Biomater. Sci. Eng. 3(12) (2017) 3687-3694.

[25] K. Christensen, Y. Huang, Study of layer formation during droplet-based 3D printing of gel structures, J. Manuf. Sci. Eng. 139(9) (2017) 091009.

[26] P. Moy, W. Tusit, C. Gunnarsson, Tensile deformation of ballistic gelatin as a function of loading rate, Proceedings of the XIth International Congress and Exposition June 2 (2008) 1-6.

[27] G. Subhash, Q. Liu, D.F. Moore, P.G. Ifju, M.A. Haile, Concentration dependence of tensile behavior in agarose gel using digital image correlation, Exp. Mech. 51 (2011) 255-262.

[28] T. Boland, T. Xu, B.J. Damon, B. Manley, P. Kesari, S. Jalota, S. Bhaduri, Drop on demand printing of cells and materials for designer tissue constructs, Mat. Sci. Eng. C 27 (2007) 372-376.

[29] Y. Nishiyama, M. Nakamura, C. Henmi, K. Yamaguchi, S. Mochizuki, H. Nakagawa, K. Takiura, Development of a three-dimensional bioprinter: construction of cell supporting

structures using hydrogel and state-of-the-art inkjet technology, J. Biomech. Eng. 131 (2009) 035001.

[30] J.A. Rowley, G. Madlambayan, D.J. Mooney, Alginate hydrogels as synthetic extracellular matrix materials, Biomaterials 20 (1999) 45-53.

[31] L. Fan, M. Cao, S. Gao, T. Wang, H. Wu, M. Peng, X. Zhou, M. Nie, 2013, Preparation and characterization of sodium alginate modified with collagen peptides, Carbohydr. Polym. 93 (2013) 380-385.

[32] A. Gravelle, S. Barbut, A. Marangoni, Influence of particle size and influence interactions on the physical and mechanical properties of particle filled myofibrillar protein gels, RSC Adv. 5 (2015) 723-735.

[33] T. Braschler, A. Valero, L. Colella, K. Pataky, J. Brugger, P. Renaud, Link between alginate reaction front propagation and general reaction diffusion theory, Anal. Chem. 83 (2011) 2234-2242.

[34] E.R. Morris, D.A. Rees, D. Thom, J. Boyd, Chiroptical and stoichiometric evidence of a specific primary dimerisation process in alginate gelation, Carbohydr. Res. 66 (1978) 145–154.

[35] J.H. Wang, Tracer-diffusion in liquids: IV. Self-diffusion of calcium ion and chloride ion in aqueous calcium chloride solutions, J. Am. Chem. Soc. 75 (1953) 1769–1770.

[36] L. Li, A.E. Davidovich, J.M. Schloss, U. Chippada, R.R. Schloss, N.A. Langrana, M.L. Yarmush, Neural lineage differentiation of embryonic stem cells within alginate microbeads, Biomaterials 32 (2011) 4489–4497.

[37] M. Mancini, M. Moresi, R. Rancini, Mechanical properties of alginate gels: empirical characterisation, J. Food Eng. 39(4) (1999) 369-378.